https://doi.org/10.5194/angeo-2019-82
Preprint. Discussion started: 13 June 2019

Annales Geophysicae Discussions

Invariants of the Spatial-Energy Structure and Modeling of the Earth's Ion Radiation Belts

Alexander S. Kovtyukh
Skobeltsyn Institute of Nuclear Physics, Moscow State University, Moscow, 119234, Russia; kovtyukhas@mail.ru

Abstract The spatial-energy distributions of proton fluxes in the Earth's radiation belts (ERB) are well studied and the NASA averaged empirical models constructed for them (the latest versions are AP8 and AP9). These models are widely used in space research. However, for heavier ERB ions (helium, oxygen, etc.), much less measurements were made on satellites, especially in the energy range from tens to hundreds of MeV, and there are no sufficiently complete and reliable models for them. Meanwhile, such ions, although there are much smaller than protons, play a very important role in the physics of ERB, especially in their dynamics, as well as in solving problems of ensuring the safety of space flights. The data on such ions represent a rather fragmentary picture, in which there are significant "white spots". Using the methods considered in this paper, these fragmentary data can be streamlined, linked to each other and get a regular picture that has a simple physical meaning. Spatial-energy distributions of the stationary fluxes of protons, helium ions and ions of the CNO group with energy from 100 keV to 200 MeV at $L \sim 1$–8 considered here on the data of the satellites for 1961–2017. It is found, that results of the measurements of the ion fluxes are arrange in certain regular patterns in the spaces $\{E, L\}$ and $\{L, B/B_0\}$. This effect connected with the existence of invariant parameters of these distributions of ion fluxes. These invariant parameters are very useful and necessary for constructing the ion models of the ERB. The physical mechanisms leading to formation spatial-energy structure of the ERB ion fluxes and the values of its invariant parameters discussed here. In the course of this work, solar-cyclic (11-year) variations in the distributions of helium and carbon-nitrogen-oxygen ions fluxes in the ERB studied for the first time. It shown that, as compared with such variations in the proton fluxes studied earlier, the amplitude of the variations of heavier ions is much larger and increases with increasing their mass.

Keywords. Magnetospheric physics (energetic particles trapped)

https://doi.org/10.5194/angeo-2019-82
Preprint. Discussion started: 13 June 2019

Annales Geophysicae Discussions

1 Introduction

The Earth's radiation belts (ERB) consist of charged particles with energy from E ~ 100 keV to several hundreds of MeV. They trapped by the geomagnetic field at altitudes from ~ 200 km to ~ 50–70 thousands kilometers. The ERB consist mainly of electrons and protons. In the ERB there are also ions of helium, oxygen, and other elements with the atomic number $Z \geq 2$ (Z is the charge of the atomic nucleus with respect to the charge of the proton). Fluxes of ions and its distributions vary during geomagnetic disturbances. These fluxes depend also on the phase of the solar cycle, conditions in the interplanetary space, and other factors.

Particles with different energy and with different pitch-angles α (α is the angle between the local vector of the magnetic field and vector of the particle velocity) which injected into some point of the geomagnetic trap, drifting with conservation of the invariants μ and K gradually populate a narrow layer around the Earth, so-called drift shell (Alfvén and Fälthammar, 1963; Northrop, 1963). Therefore, experimental data on the ERB most simply represented in coordinates $\{L, B\}$, where L is a parameter of a drift shell and B is the local induction of a magnetic field (McIlwain, 1961). For a dipole magnetic field parameter L is a distance, in the equatorial plane, from the given magnetic field line to the center of the dipole (in the Earth's radii R_E).

Outer and inner regions of the ionic ERBs formed and maintained in dynamic equilibrium with the environment by the various mechanisms (see review Kovtyukh, 2018).

The outer belt ($L > 3$) of ions is formed mainly by the mechanisms of radial diffusion of the particles of the hot plasma from the periphery regions of the magnetosphere into the geomagnetic trap under the action of low-frequency fluctuations of electric and magnetic fields which resonate with drift periods of the trapped particles. This transport accompanied by betatron acceleration of ions, and by ionization losses and charge exchange of ions with atoms of the residual atmosphere.

The inner belt ($L < 2.5$) of protons with $E > 10$ MeV is forming mainly as result of decay of neutrons knocked from the atomic nuclei of the atmosphere by the Galactic Cosmic Rays. For protons with $E < 10$ MeV, this mechanism (CRAND) supplemented by the radial diffusion of particles from the outer to the inner belt. The inner belt of ions with $Z > 4$ formed mainly from ions of the Anomalous component of Cosmic Rays (ACR).

In the intermediate region ($2.5 < L < 3.5$) during strong magnetic storms is operated also the mechanism of capture ions from the Solar Cosmic Rays (see, e.g., Selesnick et al., 2014).

Thus, the main mechanisms of formation of the ERB, sources and losses of these ions we know. However, for the comprehensive verification of the physical models and to identification of the mathematical models parameters it is necessary primarily to create sufficiently complete and reliable empirical models of the ERB for each ion component.

These models one can create only on the base of experimental data obtained over many years and decades. Such models (see, e.g., Ginet et al., 2013) created for protons (AP8/AP9). However, measurements of fluxes of ions with $Z \geq 2$ represent a difficult technical problem, due to the small fluxes of these ions and high background fluxes of protons and electrons. We facing here with the problems of limited and incomplete information. Therefore, sufficiently complete empirical models of the ERB for ions with $Z \geq 2$, similar to models for protons, we do not have, although there are separate fragments of empirical and semi-empirical models for these ions. For example, such models presented for the oxygen ions trapped in the ERB from the ACR (Selesnick et al., 2000; Selesnick, 2001).

When constructing such models, it is necessary to coordinate the data of various experiments. More or less significant discrepancies in the results of these experiments connected with differences in the construction of instruments and in the trajectories of the satellites, differences in the energy ranges and in the angular characteristics of the instruments, differences in the phase of the solar cycle, and with many other physical factors. These factors influence on the fluxes of ions with $Z \geq 2$ in the ERB more significantly than on the proton fluxes (see, e.g., Kovtyukh, 2018).

https://doi.org/10.5194/angeo-2019-82
Preprint. Discussion started: 13 June 2019

The creation of the ERB models for ion with $Z \geq 2$ is also necessary in connection with estimates of the radiation hazard of space flights for humans and with the widespread introduction of new radiation-sensitive technologies into the space equipment.

This paper consider some approaches to solving the problem of creation of the empirical models of the ERB for ions with $Z \geq 2$ and presents the first model versions of the stationary ERB for helium ions and for ions of the CNO group in the range $E \sim 0.1$–100 MeV/nucleon at $L \sim 2$–6.

In the following sections, we consider the experimental data on the spatial-energy structure of the ERB for protons, helium ions and ions of the CNO group. We consider invariants of the structure of the ERB (Sect. 2), distributions of ion fluxes in the spaces $\{E, L\}$ and $\{L, B/B_0\}$ and solar-cyclic variations of these distributions (Sect. 3), physical mechanisms of these structure formation and the values of its invariant parameters (Sect. 4). Section 5 concludes the paper.

2 Invariants of the ion Earth's radiation belts structure

Five invariant parameters of the stationary distributions of the ERB ions in the range $\mu = 0.01$–50 keV/nT at $L > 2$–3 were found as result of cross-analysis of satellite's data in (Kovtyukh, 1984, 1985a, 1985b, 1989, 1999a). For this analysis were used data of the satellites Explorer-12 (1961), Explorer-14 (1962), Injun-4 (1965–1966), Explorer-33 (1966), Injun-5 (1968), ESRO-2 (1968), 1968-26B (1968), OVI-19 (1969), Molniya-1 (1970–1974), Explorer-45 (1971–1972), 1972-076B (1972–1973), ATS-6 (1974), Molniya-2 (1975), ISEE-1 (1977–1979), SCATHA (1979), AMPTE/CCE (1984-1986), Gorizont-21 (1985-1986), Akebono (1989-1991), CRRES (1991), Gorizont-35 (1992) and ETS-VI (1994).

Invariant parameters of the ERB ion fluxes structure include the following quantities:

μ_m is corresponds to maximum at $E_m(L)$ in the energy spectra (exist only for solar origin ions);

μ_0 is corresponds to index $E_0(L)$ of the exponential part of the energy spectra at $E_m < E < E_b$: $J \propto \exp(-E/E_0)$;

μ_b is corresponds to the boundary E_b between exponential spectral segment and a power-law tail;

γ is corresponds to exponent of the power-law tail of the energy spectra: $J \propto E^{-\gamma}$;

ξ_i is corresponds to the ratio of parameters μ_m, μ_0, or μ_b for different ion components (scaling parameter).

Specific values of μ_m and μ_b depends on geomagnetic and solar activity; sometimes the segment $\mu_m < \mu < \mu_b$ degenerates, but usually it is clearly expressed and well approximated by the exponent function.

These parameters of the ions radiation belts are invariants relatively L shells, and are displayed not only in the energy spectra, but also in all other ion distributions by E, L and B/B_0 for all main ion components of the ERB. Here B and B_0 are values of the magnetic field at the point of measurement and in the equatorial plane on the same L shell. For each of the main ion components of the ERB it was established that spatial, energy and pitch-angle distributions of fluxes are connected to each other with by means of the invariant parameters μ_m, μ_0, μ_b, γ and ξ_i (Kovtyukh, 1984, 1994, 1999a, 2001). These parameters are completely determines the spatial-energy structure of the ERB ion fluxes in a wide region of the space $\{\mu, L\}$.

For protons with equatorial pith-angles $\alpha_0 = 90 \pm 50^{\circ}$, these parameters have the following values:

$$\mu_m = 0.55 \pm 0.10 \text{ keV/nT},$$

$$\mu_b = 1.16 \pm 0.29 \text{ keV/nT},$$

$$\mu_0 = 0.29 \pm 0.10 \text{ keV/nT, for } \mu_m < \mu < \mu_b,$$

$$\gamma = 4.25 \pm 0.75, \text{ for } \mu > \mu_b.$$

https://doi.org/10.5194/angeo-2019-82
Preprint. Discussion started: 13 June 2019

Annales Geophysicae Discussions

For helium ions and for CNO group ions with $\alpha_0 = 90 \pm 50^{\circ}$ these parameters have following values:

$$\mu_m/\xi_i = 0.5 \pm 0.2 \text{ keV/nT},$$

$$\mu_b/\xi_i = 1.4 \pm 0.8 \text{ keV/nT},$$

$$\mu_0/\xi_i = 0.3 \pm 0.2 \text{ keV/nT, for } \mu_m/\xi_i < \mu/\xi_i < \mu_b/\xi_i,$$

$$\gamma = 4.7 \pm 2.2, \text{ for } \mu/\xi_i > \mu_b/\xi_i.$$

According to Kovtyukh (1985a, 1985b, 1989, 1999a), parameters μ_0, μ_b and γ applicable for ion distributions only at $L > 3$, and parameters μ_m and ξ_i applicable only at $L > 3.5$. Such restrictions connected with the ionization losses of ions.

The scatter of the values of these parameters exceed considerably the statistical errors of the measurements and it is connected with the averaging the experimental data of many satellites for thirty years. These measurements obtained in different phases of the solar activity, in different ranges of E, α_0, L and B/B_0, by different devices which have different resolution, different periods of accumulation and averaging of the data.

From minimum to maximum of solar activity, ξ_i changes from M_i to Q_i (M_i and Q_i are a mass and charge of ions with respect to the corresponding values for protons), the exponential segment of the spectra become softer (μ_0/ξ_i decreases in 1.5–2.0 times), and μ_b/ξ_i increases slightly (Kovtyukh, 1999a).

Parameter γ depends slightly on B/B_0, but μ_m, μ_0 and μ_b decreases with increasing B/B_0 at $L <$ 6.6.

Usually, $\mu_b \approx \gamma\mu_0$ (the exponential and the power-law parts of the spectrum smoothly transfer one into other) and $\mu_m \neq \mu_0$. Since for the Maxwellian distributions $\mu_m = \mu_0$ and parameter ξ_i should be close to unity, which does not correspond to the experimental results, an exponential part of the ion spectra, as well as a power-law tail, are non-equilibrium.

The simplest explanation of the exponential segment and maximum in the spectra of the ERB ions is that they reflect, in some degree, the quasi-Maxwellian distributions of the ions in the solar wind, the main source of the ERB ions. The power-law tail of the ions ERB spectra formed, most likely, by statistical mechanisms of particle acceleration in the magnetosphere (see Sect. 4 for more details).

3 Modelling of the spatial-energy structure of ion fluxes in the radiation belts

As examples of modeling of the ERB for ions with $Z \geq 2$, in this section are presented the distributions of the fluxes of helium ions and ions of the CNO group in the spaces of variables $\{E, L\}$ and $\{L, B/B_0\}$. Such presentations of fragmentary experimental data obtained in different ranges of E, L and B/B_0 are the most capacious envelopes of these data and make it possible to organize them most effectively. For comparison, there are presented also the distributions of the fluxes of protons of the ERB, which constructed by the same method. All of these distributions based on the satellite data averaged for quiet periods.

For these distributions, only reliable data on ion fluxes were used which obtained in those regions of E, L and B/B_0 where these fluxes not distorted by the background of other particles. For helium ions and for CNO group ions one have much smaller such data than for protons. In many important experiments, the instruments did not allow separate fluxes of ions with $Z \geq 2$ by charge of ions. For ions of the CNO group, separation by mass also were not performing usually. For heavier ions, for example for Fe ions, we have even smaller such data. Therefore, this paper

https://doi.org/10.5194/angeo-2019-82
Preprint. Discussion started: 13 June 2019

presents only helium ions (without separating them by charge) and ions of CNO group (without separating them by mass and charge).

Figures 1–6 shows the experimental results for differential fluxes of protons, helium ions, and ions of the CNO group in the ERB near the plane of the geomagnetic equator, averaged for quiet geomagnetic conditions and presented in space $\{E, L\}$. The values E and L presented in the logarithmic scales. The ion fluxes J have a dimension (cm^2 s ster MэB/n)$^{-1}$ and corresponds to the energies E (MeV/n) and the equatorial pitch-angle $\alpha_0 \sim 90^o$. In some cases in these figures, an average ion energies in the instrument channels corrected for the steepness of corresponding energy spectra. For the data on these figures, lines of equal intensity of ion fluxes are plotted (by the least squares method), and a decimal logarithms of the fluxes are shown near each line.

There can be trapped on the drift shell only ions with energy less than some maximum values determining by the Alfvén's criterion: $\rho_i(L, E, M_i, Q_i) << R_c(L)$, where ρ_i is the gyroradius of ions, and R_c is the radius of curvature of the magnetic field near the equatorial plane. According to this criterion and the theory of stochastic motion of particles, a geomagnetic trap can capture and durably hold only ions with E (MeV) < $2000\times(Q_i^2/M_i)\ L^{-4}$ (Ilyin et al., 1984). This boundary, for protons and atomic nuclei, presented in Figs. 1–6 by the green line.

Figures 1 and 2 shows exp results for proton fluxes in space $\{E, L\}$ averaged for quiet periods.

Figure 1 presents a results of the satellites 1968-81A (Stevens et al., 1970), Injun-5 (Krimigis, 1970; Venkatesan and Krimigis, 1971; Pizzella and Randall, 1971), OV1-19 (Croley et al., 1976), Azur (Hovestadt et al., 1972; Westphalen and Spjeldvik, 1982), Molniya-1 (Panasyuk and Sosnovets, 1973), GEOS-2 (Wilken et al., 1986), CRRES (Albert et al., 1998; Vacaresse et al., 1999), GEO-3 (Selesnick et al., 2010) and Van Allen Probes (Selesnick et al., 2014, 2018), obtained near maxima of solar activity in 20th, 22th, 23th and 24th solar cycles (1968–1971, 1990–1991, 2000, 2012–2017).

Figure 2 presents a results of the satellites Relay-1 (Freden et al., 1965), OHZORA, ETS-VI and Akebono (Goka et al., 1999), obtained near minima of solar activity between 19th and 20th, 21th and 22th, 22th and 23th solar cycles (1963, 1984–1985, 1994–1996).

The data of the satellites Explorer-45 (Fritz and Spjeldvik, 1979, 1981; Spjeldvik and Fritz, 1983) and ISEE-1 (Williams, 1981; Williams and Frank, 1984) refer to the years with intermediate solar activity (1971–1972, 1977–1978) and at $L > 2.5$ are used in Figs. 1 and 2. The dependence of proton fluxes on solar activity variations rapidly decreases with increasing L, and at $L > 2$ these variations practically does not show in the satellite data (see, e.g., Vacaresse et al., 1999).

From the comparison of Figs. 1 and 2, one cand an see that at $L < 2.5$, and especially on $L < 1.4$, the proton fluxes in the minima of solar-cyclic variations (Fig. 2) are higher than in the maxima of solar activity (Fig. 1). Moreover, at the minima of solar activity, the inner edge of a proton flux radial profiles with $E > 1$ MeV is less steep and achieves smaller L shells.

Solar-cyclic (11-year) variations of proton fluxes with $E > 1$ MeV in the inner region of the ERB connected mainly with the variations in the concentrations of atoms in the atmosphere (see, e.g., Pizzella et al., 1962; Hess, 1962; Blanchard and Hess, 1964; Filz, 1967; Nakano and Heckman, 1968; Vernov, 1969; Dragt, 1971; Huston et al., 1996; Vacaresse et al., 1999; Kuznetsov et al., 2010; Qin et al., 2014). These variations achieves one order of magnitude at L = 1.14 and reduced rapidly with increasing L (see, e.g., Vacaresse et al., 1999). The shape of the proton energy spectra also undergo by solar-cyclic variations in the inner region of the ERB.

The atmospheric density depends on the intensity of the ultraviolet radiation of the Sun and determines the loss rates of the ERB protons. Decreases in the amplitude of these variations with L is connected with increases in the lifetime of protons with increasing L; at $L > 2$, this time approach to the main period of the solar cycle. In these variations expressed some inertness of the changes in the atmospheric density, and this lag increases with increasing L.

In Figs. 1 and 2, the red line shows the proton energy values corresponding to the average value of the invariant μ_b, and the blue line corresponds to the average value of the invariant μ_m; these

https://doi.org/10.5194/angeo-2019-82
Preprint. Discussion started: 13 June 2019

Annales Geophysicae Discussions

values obtained from experimental data in (Kovtyukh, 1984, 1985a, 1985b, 1989, 1999a) and presented in Sect. 2. These lines do not distinguished in Figs. 1 and 2, since the solar-cyclic variations of the ion fluxes in the outer belt (at $L > 2.5$) are significantly weaker than in the inner belt (see, e.g., Vacaresse et al., 1999). The maximum deviations from the mean values of μ_b and μ_m plotted on the red and blue lines with vertical segments; on a logarithmic scale, the magnitudes of these segments do not depend on L shell.

The isolines of the proton fluxes in Figs. 1 and 2, at $L > 3$ above the red line ($\mu > \mu_b$), go almost parallel to it and are separated from each other approximately equal distances on a logarithmic scale of energy. This conforms to adiabatic transformations of fluxes for the energies corresponding to the power-law tail of the proton spectra. It results from these figures that in the region of a near-dipole magnetic field, at L = 3–6, the parameter $\gamma = 4.8 \pm 0.5$. At $L > 6$, the distance between these isolines increases with L, and the parameter γ decreases, from ~ 4.7–5.0 at L = 6 to ~ 4.1–4.5 at L = 8. This is due to the deviation of the magnetic field from the dipole configuration (L shells correspond here to the dipole magnetic field), as well as to the increasing variability of this field with increasing L. In the interval between the red and blue lines ($\mu_m < \mu < \mu_b$), the spectra have a close to exponential form and corresponds to $\mu_0 \sim 0.32$ keV/nT.

Thus, the values of the invariant parameters μ_b, μ_0 and γ of the proton flux distributions in the ERB, obtained from Figs. 1 and 2, are in good agreement with the values of these parameters given in Sect. 2 and obtained in (Kovtyukh, 1985a, 1985b, 1989, 1999a) by other methods and with other set of the experimental data.

However, a data representation, accepted here, does not allow determine the values of the parameter μ_m for protons of the ERB and compare these with the values given in Sect. 2. For this, it is necessary to reduce the step between the isolines of the fluxes ($\Delta\log J$) of protons with $E < 1$ MeV at $L > 3.5$ by ~ 10 times, which leads to significant systematic errors in such representation of the data.

In addition, it must take into account that the ionization loss mechanisms generates in the proton spectrum of the ERB also a less energetic maximum at $L < 5.5$ (this maximum considered in details in Kovtyukh, 1989). Its energy increases from ~ 0.01–0.03 MeV at L = 5.3 to ~ 0.4 MeV at L = 3.2 (the values of the adiabatic maximum on these L are ~ 0.11 MeV and ~ 0.52 MeV, respectively). These two maxima in the spectra of protons at L ~ 3–5 separated by a small local minimum and, at insufficiently high resolution of the spectrometers, have a view an extended plateau in the spectra.

According to the experimental data considered in (Kovtyukh, 1985a, 1985b, 1999a), it was found that the parameters μ_b and γ are detected only at $L > 3$. Here are considered more complete data of satellites, and these parameters for protons with $E > 10$ MeV can be traced to $L \sim 2$: at $L = 2$, $\gamma = 4.7 \pm 1.3$ (Fig. 1) and $\gamma = 4.4 \pm 0.6$ (Fig. 2). This is due to the fact that, compare with (Kovtyukh, 1985a, 1985b, 1999a), the energy range here is significantly extended toward higher energies, but the ionization losses rapidly decreases with increasing of the energy of the ERB protons (see, e.g., Schulz and Lanzerotti, 1974; Kovtyukh, 2016a, 2016b).

Figure 2 show that at very high energies the proton spectra tail becomes steeper, which corresponds to the limit of the magnetic confinement of protons in the ERB.

Figures 3 and 4 show averaged stationary fluxes of helium ions in the space $\{E, L\}$.

Figure 3 presented the data of the satellites OV1-19 (Blake et al., 1973; Fennell and Blake 1976), Explorer-45 (Fritz and Spjeldvik, 1978, 1979; Spjeldvik and Fritz, 1981) and SCATHA (Blake and Fennell, 1981; Chenette et al., 1984), obtained near maxima of solar activity in 20th and 21th solar cycles (1968–1971, 1979).

Figure 4 presented the data of the satellites Molnija-2 (Panasyuk et al., 1977), Prognoz-5 (Lutsenko and Nikolaeva, 1978), ISEE-1 (Hovestadt et al., 1981) and Akebono (Goka et al., 1999), obtained near minima of solar activity between 20th and 21th and between 22th and 23th solar cycles (1975–1977, 1996).

https://doi.org/10.5194/angeo-2019-82
Preprint. Discussion started: 13 June 2019

Annales Geophysicae Discussions

From the comparison of Figs. 1–4, it can see that for helium ions with $E > 1$ MeV/n at $L \sim 2$–3 an amplitude of the solar-cyclic (11-year) variations is more than for protons. This difference connected with the ionization losses of the ERB ions: for helium ions these losses more than for protons.

In Figs. 3 and 4, the red line shows an energy of the helium ions corresponding to the average value of the invariant μ_b/ξ_i, and the blue line corresponds to the average value of the invariant μ_m/ξ_i, which are represent in Sect. 2. Here $\xi_i = Q_i$ for Fig. 3 and $\xi_i = M_i$ for Fig. 4. It was taken into account that for $E > 0.2$ MeV/n at $L < 6$ the average (main) charge of helium ions is $Q_i = +2$ (see, e.g., Spjeldvik, 1979). The maximum deviations from the mean values of μ_b/ξ_i and μ_m/ξ_i at energy scale plotted on the red and blue lines with vertical segments; on a logarithmic energy scale, the magnitudes of these segments do not depends on L shell. The isolines of the helium ions fluxes in Figs. 3 and 4 at $L > 2$ pass above the red line almost parallel to it, and average value of the parameter $\gamma \sim 5.5$.

Thus, the values of the invariant parameters of the power-law tail of the spatial-energy flux distributions of helium ions in the ERB, obtained from Figs. 3 and 4 are in good agreement with the values of these parameters given in Sect. 2 and obtained in (Kovtyukh, 1999a) by other methods and with other compositions of experimental data. To find the values of the parameters μ_m/ξ_i and μ_0/ξ_i from Figs. 3 and 4, it is necessary to reduce the step between the isolines of the ion fluxes significantly, which leads to large systematic errors in such representation of the data.

Figures 5 and 6 show the results for the average stationary fluxes of ions of the CNO group in the space $\{E, L\}$.

Figure 5 presented the data of the satellite Explorer-45 (Spjeldvik and Fritz, 1978; Fritz and Spjeldvik, 1981), obtained near maximum of solar activity in 20th solar cycle (1971–1972).

Figure 6 presented the data of the satellites ATS-6 (Spjeldvik and Fritz, 1978; Fritz and Spjeldvik, 1981) and ISEE-1 (Hovestadt et al., 1978), obtained near the minimum of the solar activity between 20th and 21th solar cycles (1974–1975, 1977).

In Figs. 5 and 6, the red line shows the CNO ions energy values corresponding to the average value of the invariant μ_b/ξ_i, and the blue line corresponds to the average value of the invariant μ_m/ξ_i, which presented in Sect. 2. Here $\xi_i = Q_i$ for Fig. 5 and $\xi_i = M_i$ for Fig. 6. It was taken into account that for $E > 0.1$ MeV/n at $L \sim 3$–5 the average charge of the CNO group ions is $Q_i = +4$ (see, e.g., Spjeldvik and Fritz, 1978). The maximum deviations from the mean values of μ_b/ξ_i and μ_m/ξ_i at energy scale plotted on the red and blue lines with vertical segments; on a logarithmic energy scale, the magnitudes of these segments do not depends on L shell. The isolines of the CNO ions fluxes in Figs. 5 and 6 at $L > 3$ pass almost parallel to each other.

However, at the maximum of solar activity their slope on $L > 3$ is significantly less than the slope of the red line, which indicates more significant ionization losses of ions of the CNO group at $L = 3$–5 compared to these losses for protons and for helium ions. According to these results, at $L \sim 3$–6 for ions of the CNO group, the average value of the parameter $\gamma \sim 6$.

Thus, the values of the invariant parameters of the power-law tail of the spatial-energy flux distributions of the CNO group ions in the ERB, obtained from Figs. 5 and 6, are in good agreement with the values of these parameters given in Sect. 2 and obtained in (Kovtyukh, 1999a) by other methods and with other set of experimental data. To find the values of the parameters μ_m/ξ_i and μ_0/ξ_i from Figs. 5 and 6, it is necessary to reduce the step between the isolines of the ion fluxes significantly, which leads to large systematic errors in such representation of the data.

As well as for protons (Figs. 1 and 2), for helium ions (Figs. 3 and 4) and CNO group ions (Figs. 5 and 6), with $E > 0.1$ MeV/n at small L, fluxes during solar minimum more, than during solar maximum. The larger the atomic number Z of the ERB ions, the greater the amplitude of these variations. The solar-cyclic variations of ion fluxes explained by the same mechanism of ionization losses of particles, which proposed for the ERB protons (see above). The main loss

https://doi.org/10.5194/angeo-2019-82
Preprint. Discussion started: 13 June 2019

Annales Geophysicae Discussions

mechanism of ions at E > 0.1 MeV/n at L < 3.5 are Coulomb losses, for which the loss rate increases rapidly with increasing Z of the ions (as Z^2).

Figs. 7–9 show the experimental results for differential fluxes of protons and helium ions in the ERB, averaged for quiet geomagnetic conditions and presented in the space {L, B/B_0} for different ion energies (as examples). The values of L and B/B_0 are plotted on logarithmic scales. For these results, the lines of equal intensity of ion fluxes are made, and decimal logarithms of the fluxes are shown near each of these line.

Figure 7 presents stationary fluxes of protons with E = 0.4 MeV, averaged for quiet periods by the data of the satellites Injun-5 (Krimigis, 1970; Venkatesan and Krimigis, 1971; Pizzella and Randall, 1971), Molniya-1 (Panasyuk and Sosnovets, 1973) and GEOS-2 (Wilken et al., 1986). These data obtained near the maxima of solar activity in 20th and 21th solar cycles (1968–1970, 1978).

Figure 8 presents stationary fluxes of protons with E = 0.4 MeV, averaged for quiet periods by the data of the satellites 1964-45A (Mihalov and White, 1966), ISEE-1 (Williams, 1981; Williams and Frank, 1984) and Polar (Walt et al., 2001). These data obtained near the minima of the solar activity between 19th and 20th, between 20th and 21th and between 22th and 23th solar cycles (1964, 1977, 1998).

From Figs. 7 and 8 it can be seen, that for protons with E = 0.4 MeV during solar activity minima fluxes are greater than during solar activity maxima, at the same points in the space {L, B/B_0}; most significantly this discrepancy in proton fluxes is observed at B/B_0 > 100 (this is also valid for other proton energies). This effect connected with the solar-cyclic variations of the Earth's upper atmosphere temperature, as for protons of the ERB near the equatorial plane.

Figure 9 presents stationary fluxes of helium ions with E = 0.2 MeV/n, averaged for quiet periods by the data of satellite Polar (Spjeldvik et al., 1999) which were obtained near the minimum of the solar activity between 22th and 23th solar cycles (1996). For equatorial plane (B/B_0 = 1) we used data of satellite Explorer-45 presented in (Fritz and Spjeldvik, 1978, 1979; Spjeldvik and Fritz, 1981).

From Figs. 7–9 it seen that with increasing B/B_0 the maximum of the ion fluxes shifts to a higher L. This performed also for other ion energies in the range of 0.1–100 MeV/n and connected with increasing in ionization losses and decreasing in the radial diffusion rate of the ERB ions with increasing B/B_0.

With decreasing altitude of the observation point (at a given L), the concentration of atoms and ionization losses increases, which lead to the formation an altitude dependence of the ion fluxes: with decreasing altitude (at fixed L and E), ion fluxes of the ERB are decreases. With decreasing L, this dependence enhances and, consequently, at low altitudes (at h ~ 500–1000 km) a maximum of the ERB should be located at larger L compared to the equatorial plane (see Figs. 7–9).

When the exosphere is heated, the altitude dependence of a concentration of atoms becomes weaker. Therefore, the difference in the position of the ERB maximum in the equatorial plane and at low altitudes decreases (see Figs. 7 and 8).

Since reliable experimental data on helium ions in the ERB are insufficient, the distributions of their fluxes in space {L, B/B_0}, especially at higher energies, have more or less significant lacunae. The most complete distributions of these ions in the space {L, B/B_0} obtained only for E < 1 MeV/n in the minimum of solar activity. On ions of the CNO group one have even less reliable and complete data. The distributions of these ions in the space {L, B/B_0} represent a very variegated picture. However, it is possible to conclude from these incomplete data that for higher helium ion energies, as well as for ions of the CNO group, the pattern of flux distribution in space {L, B/B_0} is similar in form to that shown in Figs. 7–9.

Patterns of isolines of fluxes of the ERB ions in Figs. 1–9 are almost identical in shape for various ionic components, especially for more complete data of protons and helium ions on L > 2, and with increasing E and L the degree of such similarity increases. Some deviations of these

https://doi.org/10.5194/angeo-2019-82
Preprint. Discussion started: 13 June 2019

isolines from the overall picture for ions with $Z > 2$ are mainly due to the deficiency of experimental data. This similarity has a basis in the unity of the main source (solar wind) and on the unity mechanisms of transfer, acceleration and losses of ERB ions (radial diffusion, betatron acceleration and ionization losses).

The absence of ions with $Z \geq 2$ at $L < 2$ (or very low values of these fluxes) is explained the fact that their lifetimes, determined by ionization losses, are much less than the same times for protons. Besides, for protons at $L < 2$ there is an additional source, CRAND (for more on this, see Kovtyukh, 2018).

4 Discussion

We consider here the main consequences of these results for the physics of the magnetosphere.

Since parameters μ_b and γ of the power-law tail of the ion spectra are invariant with respect to L, it can be assumed that this part of the ERB ion spectra formed in the plasma sheet (PS) in the tail of the magnetosphere which is adjacent to the geomagnetic trap. High-energy part of the ion spectra in the PS, at $R \sim 20$–40 R_E, has approximately the same shape as in the ERB and the average values of the parameters μ_b and γ are close to our estimates of these parameters for the ERB. Moreover, the proton spectra in the ERB are consistent with the PS spectra not only in form but also in absolute fluxes: they can be obtain from the PS ion spectra in result of the simplest adiabatic transformations (for more details see in Kovtyukh, 1999b, 2001).

According to the data of the satellites IMP-7, IMP-8 (Sarris et al., 1981; Lui et al., 1981) and also ISEE-1 (Christon et al., 1991) for ion spectra of the PS, the typical substorms not changed of the spectral shape and cause only parallel shift of the spectra along logarithmic axes E and J (for ions with $\mu/\xi_i > 0.5$ keV/nT). These results are point out that the time scales of the processes of formation of the power-law tail of the ion spectra in the PS far exceed the characteristic times of substorms.

Invariant parameters γ and μ_b of the power-law tail of the ion spectra reflect, apparently, the most fundamental features of the mechanisms of acceleration of ions in the tail of the magnetosphere. One can try to connect the obtained values of these parameters with the most general presentations on the mechanisms and character of ion acceleration in the PS of the magnetospheric tail.

Most likely, the tail of ion energy spectra of the PS formed by statistical mechanisms of the ion acceleration. This supported by many experimental results.

Statistical character of these mechanisms reveal itself, in particular, in the fact that the ratios of fluxes (and partial concentrations) of ions with different Z at low and high energies can differ greatly. During wandering in phase space, ions gradually forget their origin, and, therefore, the high-energy tails of the ion spectra do not contain unambiguous information on the partial concentrations of different components of ions in there source (for more details, see Kovtyukh, 1999b, 2001).

Most likely, the high-energy part of the ion spectra of the PS formed by the mechanisms of acceleration of particles on magnetic irregularities moving relative to each other (Fermi mechanism). If mass of the ions are small compare to masses of the magnetic irregularities in the PS, the average values of the exponent γ of the power-law tail of the spectra should not depend on mass and charge of these ions.

Under equilibrium conditions, this parameter determined by the average fraction $\bar{\beta}$ of energetic ions in the total energy density of particles and magnetic irregularities. From the theory developed on these fundament by Ginzburg and Syrovatskii (1964), it follows: $\gamma - 1 \approx (1 - \bar{\beta})^{-1}$. With increasing $\bar{\beta}$ in the interval $0 < \bar{\beta} < 1$, the value γ monotonically increases and $\gamma \to \infty$ for $\bar{\beta} \to 1$. For real average values $\bar{\beta}$ in the central PS, we get $\gamma \sim 3.5$–7.0 ($\gamma \sim 4.3$ at $\bar{\beta} \sim 0.7$).

https://doi.org/10.5194/angeo-2019-82
Preprint. Discussion started: 13 June 2019

Annales Geophysicae Discussions

Compared with the power-law tail, a short quasi-exponential segment of the ion spectra allows several different interpretations. Remaining within the framework of the most general physical concepts about the mechanisms of acceleration of cosmic plasma particles, the presence of this segment in the ion spectra of the PS and ERB one can explain in the terms of the quasi-particles theory. The structure of the magnetic field of the PS one can represent as quasi-periodic spatial grilles with different periods nested into each other (fractality) and as an energy of ions increases, grilles with more and more long periods gradually fall out from the process of acceleration of ions. Then the upper boundary of the exponential segment of the spectra corresponds to ions for which all small-scale grilles are transparent: ions with $\mu > \mu_b$ detect only the most large-scale grille. The fractal topology of the PS on scales from ~ 0.4 to ~ 8 thousand km reveal itself, for example, in the results of the satellite Geotail (Milovanov et al., 1996).

Spectra with a power-law tail and a quasi-exponential segment at lower energies generate when a value $\Delta B/\overline{B}$ for magnetic irregularities is proportional to their size δr and at $\delta r < r_s$ the spectral density of irregularities rapidly decreases with increasing δr, and at $\delta r > r_s$ remains almost unchanged. Apparently, the spectrum of magnetic irregularities in PS with thickness r_s has just such form.

Then the lower boundary μ_b of the power-law tail corresponds to the condition $r_s/\rho_i \sim 10$ (ρ_i is the gyroradius of ions), i.e. $\mu_b \sim 0.02(Q_i^2/M_i)B_s r_s^2$ keV/nT, where B_s is the average magnetic field induction in the PS (in nT) and r_s is normalized to the Earth's radius. Believing $B_s \sim 30$ nT and $r_s \sim 1.3\ R_E$, one obtain $\mu_b \sim 1.0\ (Q_i^2/M_i)$ keV/nT (for details, see Kovtyukh, 1999b).

Thus, the main invariant parameters of the ERB structure one can relate with the average physical properties of the PS.

Parameter γ one can relate with the fraction of energetic ions in the total energy density of particles and of a magnetic irregularities in the PS (Kovtyukh, 1999b, 2001).

Parameter μ_b one can relate with a thickness of the PS and a magnitude of its magnetic field (Kovtyukh, 1999b, 2001).

Parameter μ_0 one can relate with a small-scale structure (spectrum of turbulence) of the PS (Kovtyukh, 1999b, 2001).

Parameter μ_m is well corresponded to maximum in the PS ion spectra and in solar wind (Kovtyukh, 1989, 2001).

5 Conclusions

In this work, it was found that results of the measurements of the stationary fluxes of the main ion components of the ERB (protons, helium ions and ions of the CNO group) line up in the certain regular patterns in the spaces $\{E, L\}$ and $\{L, B/B_0\}$. It is reveal that such patterns is associated with the existence of invariant parameters of the spatial-energy distributions of the ERB ion fluxes and the values of these parameters are determined.

Earlier, the results of systematization of the spatial-energy distributions of the main ionic components of the ERB and finding of their invariant parameters were presents in (Kovtyukh, 1985a, 1985b, 1999a, 2001). Here, the experimental database is significantly expanded, many modern measurements of the ion fluxes of the ERB have been added, and all results are presented in a more general and visual form.

Solar-cyclic (11-year) variations of the spatial-energy distributions of the ERB ion fluxes and their invariant parameters are considered. It is shown that the larger an atomic number Z of the ERB ions, the greater the amplitude of these variations. This is also typical for faster variations in the fluxes of the ERB ions, during geomagnetic storms and other disturbances of the Earth's magnetosphere, which is underlined in the review (Kovtyukh, 2018).

https://doi.org/10.5194/angeo-2019-82
Preprint. Discussion started: 13 June 2019

Annales Geophysicae Discussions

The results presented here show that when constructing realistic multicomponent models of the ERB ion fluxes based on limited and incomplete experimental data, the invariant parameters of the ion distributions of the ERB can serve as a pattern of these fluxes distributions.

Our drawings have also revealed the localization of "white spots", especially extensive for ions with $Z \geq 6$, which should be filled on the results of the future experiments on the satellites.

The physical mechanisms leading to the formation of the invariant structure of the ERB are considered. It is shown that energy spectra of the ERB ions with μ/ξ_i > 0.5 keV/nT can be generated in the plasma sheet (PS) of the tail of the Earth's magnetosphere. In the geomagnetic trap these spectra transforms adiabatically, and ions are loss part of their energy by ionization and other loss mechanisms.

Acknowledgements This work was supported by Russian Foundation for Basic Research RFFI grant No. 17-29-01022.

References

Alfvén, H., and Fälthammar, C.-G.: Cosmical Electrodynamics, Fundamental Principles, Clarendon Press, Oxford, 1963.

Albert, J. M., Ginet, G. P., and Gussenhoven, M. S.: CRRES observations of radiation belt protons, 1, Data overview and steady state radial diffusion, J. Geophys. Res., **103**(A5), 9261–9273. https://doi.org/10.1029/97JA02869, 1998.

Blake, J. B., and Fennell, J. F.: Heavy ion measurements in the synchronous altitude region, Planet. Space Sci., **29**(11), 1205–1213, https://doi.org/10.1016/0032.0633(81)90125-2, 1981.

Blake, J. B., Fennell, J. F., Schulz, M., and Paulikas, G. A.: Geomagnetically trapped alpha particles, 2, The inner zone, J. Geophys. Res., **78**(25), 5498–5506, https://doi.org/10.1029/JA078i025p05498, 1973.

Blanchard, R. C., and Hess, W. N.: Solar cycle changes in inner-zone protons, J. Geophys. Res., **69**(19), 3927–3938, https://doi.org/10.1029/JZ069i019p03927, 1964.

Chenette, D. L., Blake, J. B., and Fennell, J. F.: The charge state composition of 0.4–MeV helium ions in the Earth's outer radiation belts during quiet times, J. Geophys. Res., **89**(A9), 7551–7555, https://doi.org/10.1029/JA089iA09p07551, 1984.

Christon, S. P., Williams, D. J., Mitchell, D. G., Huang, C. Y., and Frank, L. A.: Spectral characteristics of plasma sheet ion and electron populations during disturbed geomagnetic conditions, J. Geophys. Res., **96**(A1), 1–22, https://doi.org/10.1029/90JA01633, 1991.

Croley, D. R., Jr., Schulz, M., and Blake, J. B.: Radial diffusion of inner-zone protons: Observations and variational analysis, J. Geophys. Res., **81**(4), 585–594, https://doi.org/10.1029/JA081i004p00585, 1976.

Dragt, A. J.: Solar cycle modulation of the radiation belt proton flux, J. Geophys. Res., **76**(10), 2313–2344, https://doi.org/10.1029/JA076i010p02313, 1971.

Fennell, J. F., and Blake, J. B.: Geomagnetically trapped α-particles, Magnetospheric Particles and Fields, edited by: McCormac, B. M., D. Reidel, Dordrecht, Holland, 149–156, 1976.

Filz, R. C.: Comparison of the low-altitude inner-zone 55-MeV trapped proton fluxes measured in 1965 and 1961–1962, J. Geophys. Res., **72**(3), 959–963, https://doi.org/10.1029/JZ072i003p00959, 1967.

Freden, S. C., Blake, J. B., and Paulikas, G. A.: Spatial variation of the inner zone trapped proton spectrum, J. Geophys. Res., **70**(13), 3113–3116, https://doi.org/10.1029/JZ070i013p03113, 1965.

Fritz, T. A., and Spjeldvik, W. N.: Observations of energetic radiation belt helium ions at the geomagnetic equator during quiet conditions, J. Geophys. Res., **83**(A6), 2579–2583, https://doi.org/10.1029/JA083iA06p02579, 1978.

https://doi.org/10.5194/angeo-2019-82
Preprint. Discussion started: 13 June 2019

Annales Geophysicae Discussions

Fritz, T. A., and Spjeldvik, W. N.: Simultaneous quiet time observations of energetic radiation belt protons and helium ions: The equatorial α/p ratio near 1 MeV, J. Geophys. Res., **84**(A6), 2608–2618, https://doi.org/10.1029/JA084iA06p02608, 1979.

Fritz, T. A., and Spjeldvik, W. N.: Steady-state observations of geomagnetically trapped energetic heavy ions and their implications for theory, Planet. Space Sci., **29**(11), 1169–1193, https://doi.org/10.1016/0032-0633(81)90123-9, 1981.

Ginzburg, V. L., and Syrovatskii, S. I.: The Origin of Cosmic Rays, Pergamon Press, Oxford, 1964.

Ginet, G. P., O'Brien, T. P., Huston, S. L., Johnston, W. R., Guild, T. B., Friedel, R., Lindstrom, C. D., Roth, C. J., Whelan, P., Quinn, R. A., Madden, D., Morley, S., and Su, Yi-J.: AE9, AP9 and SPM: New models for specifying the trapped energetic particle and space plasma environment, Space Sci. Rev., **179**(1–4), 579–615, https://doi.org/10.1007/s11214-013-9964-y, 2013.

Goka, T., Matsumoto, H., and Takagi, S.: Empirical model based on the measurements of the Japanese spacecrafts, Radiation Measurements, **30**(5), 617–624, https://doi.org/10.1016/S1350-4487(99)00237-1, 1999.

Hess, W. N.: Discussion of paper by Pizzella, McIlwain, and Van Allen, 'Time variations of intensity in the Earth's inner radiation zone, October 1959 through December 1960', J. Geophys. Res., **67**(12), 4886–4887, https://doi.org/10.1029/JZ067i012p04886, 1962.

Hovestadt, D., Häusler, B., and Scholer, M.: Observation of energetic particles at very low altitudes near the geomagnetic equator, Phys. Rev. Lett., **28**(20), 1340–1343, https://doi.org/10.1103/PhysRevLett.28.1340, 1972.

Hovestadt, D., Gloeckler, G., Fan, C. Y., Fisk, L. A., Ipavich, F.M., Klecker, B., O'Gallagher, J. J., and Scholer, M.: Evidence for solar wind origin of energetic heavy ions in the Earth's radiation belt, Geophys. Res. Lett., **5**(12), 1055–1057, https://doi.org/10.1029/GL005i012p01055, 1978.

Hovestadt, D., Klecker, B., Mitchell, E., Fennell, J. F., Gloeckler, G., and Fan, C. Y.: Spatial distribution of $Z \geq 2$ ions in the outer radiation belt during quiet conditions, Adv. Space Res., **1**(1), 305–308, https://doi.org/10.1016/0273-1177(81)90125-3 , 1981.

Huston, S., Kuck, G., and Pfitzer, K.: Low-altitude trapped radiation model using TIROS/NOAA data, Radiation Belts: Models and Standards, edited by: Lemaire, J. F., Heynderickx, D., and Baker, D. N., AGU, Washington, D. C., 119–122, https://doi.org/10.1029/GM097/p0119, 1996.

Ilyin, B. D., Kuznetsov, S. N., Panasyuk, M. I., and Sosnovets, E.N.: Non-adiabatic effects and boundary of the trapped protons in the Earth's radiation belts, Bulletin of the Russian Academy of Sciences: Physics, **48**(11), 2200–2203, 1984.

Kovtyukh, A. S.: Using the magnetosphere as an analyzer of the spectra form of radiation belt particles, Geomagn. Aeron., **24**(4), 566–570, 1984.

Kovtyukh, A. S.: Relationship between the radial variation of rigidity and the form of the proton spectrum in the Earth's radiation belts, Geomagn. Aeron., **25**(1), 23–28, 1985a.

Kovtyukh, A. S.: Form of the energy spectrum of protons of the Earth's radiation belts and the mechanisms for the formation of this spectrum, Geomagn. Aeron., **25**(6), 886–892, 1985b.

Kovtyukh, A. S.: Double-peak space-energy structure of the outer ion radiation belt, Geomagn. Aeron., **29**(1), 22–26, 1989.

Kovtyukh, A. S.: Relation between the pitch angle and energy distributions of ions in the Earth's radiation belts, Geomagn. Aeron., **33**(4), 453–460, 1993.

Kovtyukh, A. S.: Solar-cycle variations of invariant parameters of ion energy spectra of the Earth's radiation belts, Cosmic Res., **37**(1), 53–64, 1999a.

Kovtyukh, A. S.: Mechanisms of formation of invariant parameters and scaling of ion spectra in a geomagnetic trap, Cosmic Res., **37**(3), 217–229, 1999b.

Kovtyukh, A. S.: Substorm dynamics of the basic parameters and mechanisms of the formation of ion spectra in the ring current, Cosmic Res., **38**(1), 38–48, 2000.

https://doi.org/10.5194/angeo-2019-82
Preprint. Discussion started: 13 June 2019

Annales Geophysicae
Discussions

Kovtyukh, A. S.: Geocorona of hot plasma, Cosmic Res., **39**(6), 527–558, https://doi:10.1023/A:1013074126604, 2001.

Kovtyukh, A. S.: Radial dependence of ionization losses of protons of the Earth's radiation belts, Ann. Geophys., **34**(1), 17–28, https://doi.org/10.5194/angeo-34-17-2016, 2016a.

Kovtyukh, A. S.: Deduction of the rates of radial diffusion of protons from the structure of the Earth's radiation belts, *Ann. Geophys*., 34(11), 1085–1098. https://doi:10.5194/angeo-34-1085-2016, 2016b.

Kovtyukh, A. S.: Ion Composition of the Earth's Radiation Belts in the Range from 100 keV to 100 MeV/nucleon: Fifty Years of Research, Space Sci. Rev., **214**(8), 124:1–124:30, https:/doi.org/10.1007/s11214-018-0560-z, 2018.

Krimigis, S. M.: Alpha particles trapped in the Earth's magnetic field, Particles and Fields in the Magnetosphere, edited by: McCormac, B. M., D. Reidel, Dordrecht, Holland, 364–379, 1970.

Kuznetsov, N. V., Nikolaeva, N. I., and Panasyuk, M. I.: Variation of the trapped proton flux in the inner radiation belt of the Earth as a function of solar activity, Cosmic Res., **48**(1), 80–85, https://doi.org/10.1134/S0010952510010065, 2010.

Lui, A. T. Y., and Krimigis, S. M.: Several features of the earthward and tailward streaming of energetic protons (0.29–0.5 MeV) in the Earth's plasma sheet, J. Geophys. Res., **86**(A13), 11173–11188, https://doi.org/10.1029/JA086iA13p11173, 1981.

Lutsenko, V. N., and Nikolaeva, N. S.: Relative content and the range of alpha particles in the inner radiation belt of the Earth by measurements on satellite Prognoz-5, Cosmic Res., **16**(3), 459–462, 1978.

McIlwain, C. E.: Coordinate for mapping the distribution of magnetically trapped particles, J. Geophys. Res., **66**(11), 3681–3691, https://doi.org/10.1029/JZ066i011p03681, 1961.

Mihalov, J. D., and White, R. S.: Low-energy proton radiation belts, J. Geophys. Res., **71**(9), 2207–2216, https://doi.org/10.1029/JZ071i009p02207, 1966.

Milovanov, A. V., Zelenyi, L. M., and Zimbardo, G.: Fractal structures and power low spectra in the distant Earth's magnetotail, J. Geophys. Res. Space Phys., **101**(A9), 19903–19910, https://doi.org/10.1029/96JA01562, 1996.

Nakano, G., and Heckman, H.: Evidence for solar-cycle changes in the inner-belt protons, Phys. Rev. Lett., **20**(15), 806–809, https://doi.org/10.1103/PhysRevLett.20.806, 1968.

Northrop, T. G.: The Adiabatic Motion of Charged Particles, Wiley-Interscience, NY, USA, 1963.

Panasyuk, M. I., and Sosnovets, E. N.: Differential energy spectrum of low-energy protons in the inner region of the radiation belt, Cosmic Res., **11**(3), 436–440, 1973.

Panasyuk, M. I., Reizman, S. Ya., Sosnovets, E. N., and Filatov, V. N.: Experimental results of protons and α-particles measurements with energy more 1 MeV/nucleon in the radiation belts, Cosmic Res., **15**(6), 887–894, 1977.

Pizzella, G., McIlwain, C. E., and Van Allen, J. A.: Time variations of intensity in the Earth's inner radiation zone, October 1959 through December 1960, J. Geophys. Res., **67**(4), 1235–1253, https://doi.org/10.1029/JZ0670i004p01235, 1962.

Pizzella, G., and Randall, B. A.: Differential energy spectrum of geomagnetically trapped protons with the Injun 5 satellite, J. Geophys. Res., **76**(10), 2306–2312, https://doi.org/10.1029/JA076i010p02306, 1971.

Qin, M., Zhang, X., Ni, B., Song, H., Zou, H., and Sun, Y.: Solar cycle variations of trapped proton flux in the inner radiation belt, J. Geophys. Res. Space Phys., **119**(12), 9658–9669, https://doi.org/10.1002/2014JA020300, 2014.

Sarris, E. T., Krimigis, S. M., Lui, A. T. Y., Ackerson, K. L., Frank, L. A., and Williams, D. J.: Relationship between energetic particles and plasmas in the distant plasma sheet, Geophys. Res. Lett., **8**(4), 349–352, https://doi.org/10.1029/GL008i004p0349, 1981.

Schulz, M., and Lanzerotti, L. J.: Particle Diffusion in the Radiation Belts, Springer, NY, USA, 1974.

Selesnick, R. S., Cummings, A. C., Leske, R. A., Mewaldt, R. A., Stone, E. C., and Cummings, J. R.: Solar cycle dependence of the geomagnetically trapped anomalous cosmic rays, Geophys. Res. Lett., **27**(15), 2349–2352, https://doi.org/10.1029/2000GL000049, 2000.
Selesnick, R. S.: Simulation of the anomalous cosmic ray radiation belt with atmospheric production and decay, Geophys. Res. Lett., **28**(17), 3417–3420, https://doi.org/10.1029/2001GL013383, 2001.
Selesnick, R. S., Hudson, M. K., and Kress, B. T.: Injection and loss of inner radiation belt protons during solar proton events and magnetic storms, J. Geophys. Res. Space Phys., **115**(A8), A08211, https://doi.org/10.1029/2010JA015247, 2010.
Selesnick, R. S., Baker, D. N., Jaynes, A. N., Li, X., Kanekal, S. G., Hudson, M. K., and Kress, B. T.: Observations of the inner radiation belt: CRAND and trapped solar protons, J. Geophys. Res. Space Phys., **119**(8), 6541–6552, https://doi.org/10.1002/2014JA020188, 2014.
Selesnick, R. S., Baker, D. N., Kanekal, S. G., Hoxie, V. C., and Li, X.: Modeling the proton radiation belt with Van Allen Probes Relativistic Electron-Proton Telescope data, J. Geophys. Res. Space Phys., **123**(1), 685–697, https://doi.org/10.1002/2017JA024661, 2018.
Spjeldvik, W. N.: Expected charge states of energetic ions in the magnetosphere, Space Sci. Rev., **23**(3), 499–538, https://doi.org/10.1007/BF00172252, 1979.
Spjeldvik, W. N., and Fritz, T. A.: Quiet time observations of equatorially trapped megaelectronvolt radiation belt ions with nuclear charge $Z \geq 4$, J. Geophys. Res., **83**(A9), 4401–4405, https://doi.org/10.1029/JA083iA09p04401, 1978.
Spjeldvik, W. N., and Fritz, T. A.: Observations of energetic helium ions in the Earth's radiation belts during a sequence of geomagnetic storms, J. Geophys. Res., **86**(A4), 2317–2328, https://doi.org/10.1029/JA086iA04p02317, 1981.
Spjeldvik, W. N., and Fritz, T. A.: Experimental determination of geomagnetically trapped energetic heavy ion fluxes, Energetic Ion Composition in the Earth's Magnetosphere, edited by: Johnson, R. G., Terra Science, Tokyo, 369–421, 1983.
Spjeldvik, W. N., Fritz, T. A., Chen, J., and Sheldon, R. B.: POLAR spacecraft observations of helium ion angular anisotropy in the Earth's radiation belts, Ann. Geophys., **17**(6), 723–733, https://doi.org/10.1007/s00585-999-0723-z, 1999.
Stevens, J. R., Martina, E. F., and White, R. S.: Proton energy distributions from 0.060 to 3.3 MeV at 6.6 Earth radii, J. Geophys. Res., **75**(28), 5373–5385, https://doi.org/10.1029/JA075i028p05373, 1970.
Vacaresse, A., Boscher, D., Bourdarie, S., Blanc, M., and Sauvaud, J. A.: Modeling the high-energy proton belt, J. Geophys. Res. Space Phys., **104**(A12), 28601–28613, https://doi.org/10.1029/1999JA900411, 1999.
Venkatesan, D., and Krimigis, S. M.: Observations of low-energy (0.3– to 1.8–MeV) differential spectrums of trapped protons, J. Geophys. Res., 76(31), 7618–7631, https://doi.org/10.1029/JA076i031p07618, 1971.
Vernov, S. N.: The Earth's radiation belts. In G. Bozóki, E. Gombosi, A. Sebestyén, A. Somogyi (Eds.), Proc. 11th ICRC, Budapest, 85–162, 1969.
Walt, M., Voss, H. D., Lev-Tov, S. J., Mobilia, J., and Jahn, J.-M.: Diffusion of 155 to 430 keV protons in the Earth's radiation belt, J. Geophys. Res. Space Phys., **106**(A4), 5957–5966, https://doi.org/10.1029/2000JA003029, 2001.
Westphalen, H., and Spjeldvik, W.N.: On the energy dependence of the radial diffusion coefficient and spectra of inner radiation belt particles: Analytic solution and comparison with numerical results, J. Geophys. Res., **87**(A10), 8321–8326, https://doi.org/10.1029/2000JA087iA10p08321, 1982. 19_RB_I_Mod_GRL
Wilken, B., Baker, D. N., Higbie, P. R., Fritz, T. A., Olson, W. P., and Pfitzer, K. A.: Magnetospheric configuration and energetic particle effects associated with a SSC: A case study of the CDAW 6 event on March 22, 1979, J. Geophys. Res., **91**(A2), 1459–1473, https://doi.org/10.1029/JA091iA02p01459, 1986.

https://doi.org/10.5194/angeo-2019-82
Preprint. Discussion started: 13 June 2019

Williams, D. J.: Phase space variations of near equatorially mirroring ring current ions, J. Geophys. Res., **86**(A1), 189–194, https://doi.org/10.1029/JA086iA01p00189, 1981.

Williams, D. J., and Frank, L. A.: Intense low-energy ion populations at low equatorial altitude, J. Geophys. Res., **89**(A6), 3903–3911, https://doi.org/10.1029/JA089iA06p03903, 1984.

https://doi.org/10.5194/angeo-2019-82
Preprint. Discussion started: 13 June 2019

Annales Geophysicae
Discussions
Open Access

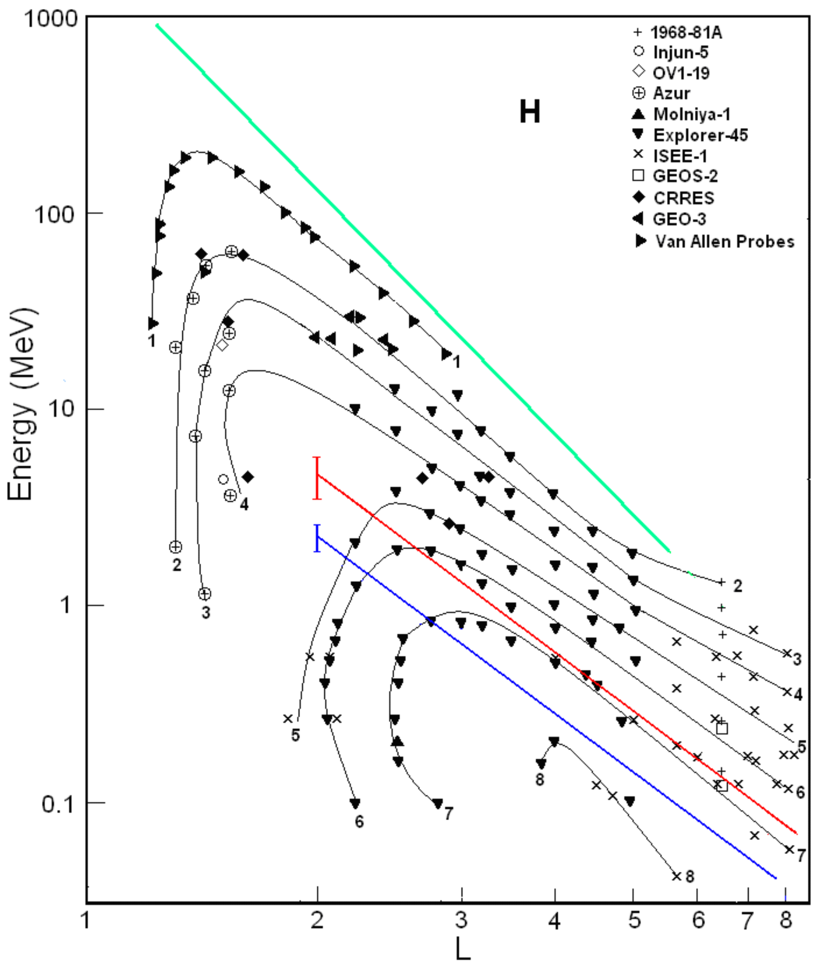

Figure 1. Proton fluxes in the ERB near maxima of a solar activity. A numbers on the curves are equal the values of a decimal logarithms of J where J in (cm^2 s ster MэB)$^{-1}$ are differential fluxes of protons with $\alpha_0 \approx 90^{o}$. The data of different satellites presented by different symbols.

https://doi.org/10.5194/angeo-2019-82
Preprint. Discussion started: 13 June 2019

Annales Geophysicae Discussions

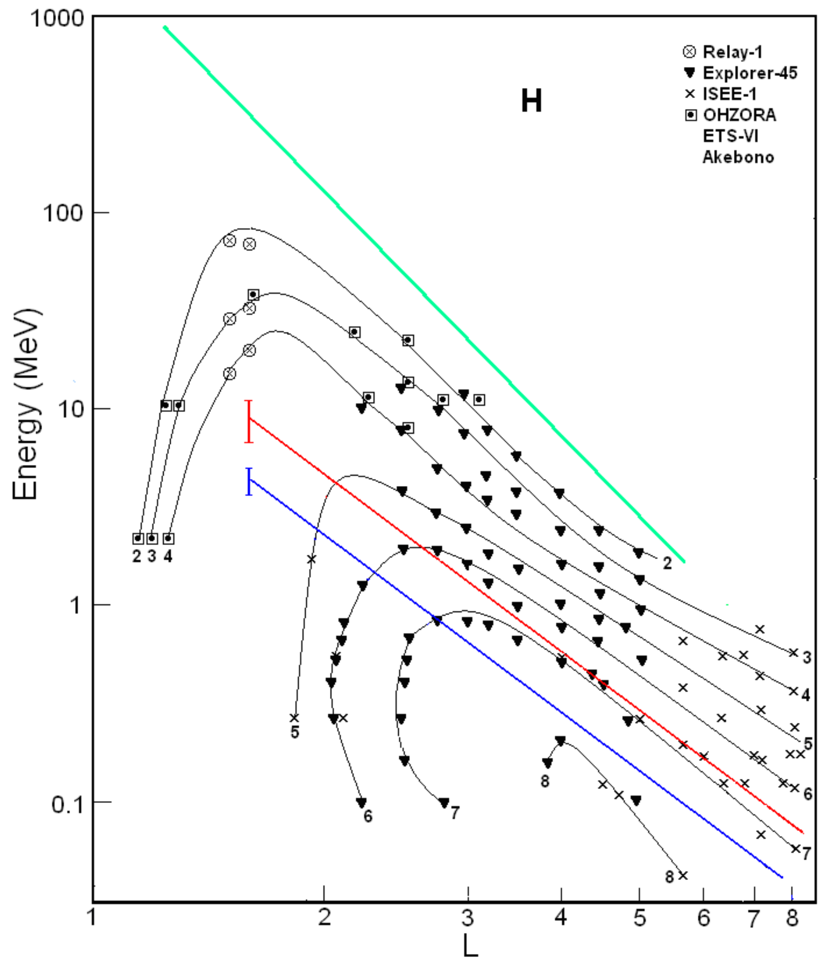

Figure 2. Proton fluxes in the ERB near minima of a solar activity. A numbers on the curves are equal the values of a decimal logarithms of J where J in (cm^2 s ster MэB)$^{-1}$ are differential fluxes of protons with $\alpha_0 \approx 90^{\circ}$. The data of different satellites presented by different symbols.

https://doi.org/10.5194/angeo-2019-82
Preprint. Discussion started: 13 June 2019

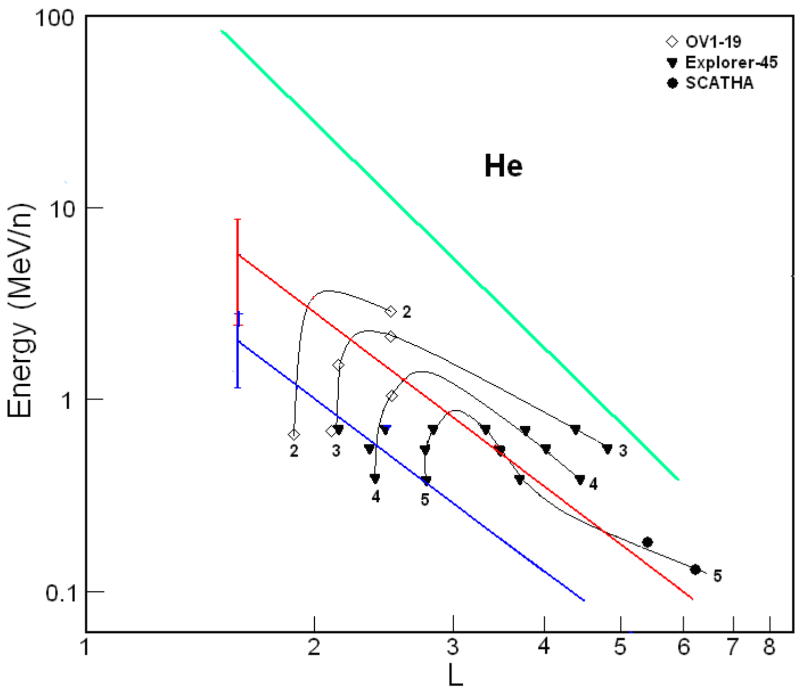

Figure 3. Helium ion fluxes in the ERB near the maxima of a solar activity. A numbers on the curves are equal the value of a decimal logarithms of J where J in (cm^2 s ster MэB/n)$^{-1}$ are differential flux of protons with $\alpha_0 \approx 90^{\circ}$ (near the plane of the geomagnetic equator). The data of different satellites presented by different symbols.

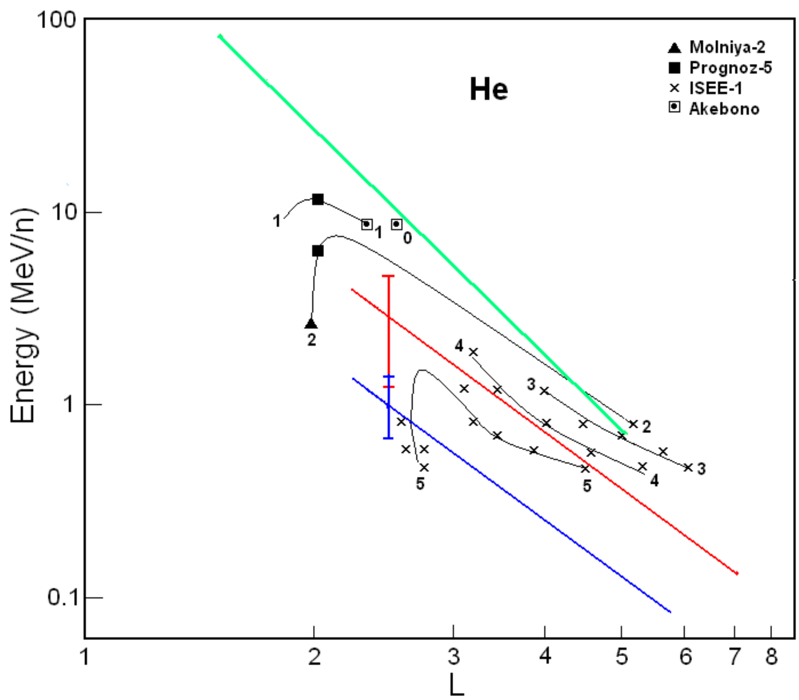

Figure 4. Helium ion fluxes in the ERB near the minima of a solar activity. A numbers on the curves are equal the values of a decimal logarithms of J where J in (cm^2 s ster MэB/n)$^{-1}$ are differential flux of protons with $\alpha_0 \approx 90^{\circ}$ (near the plane of the geomagnetic equator).The data of different satellites presented by different symbols.

https://doi.org/10.5194/angeo-2019-82
Preprint. Discussion started: 13 June 2019

Annales Geophysicae
Discussions
Open Access

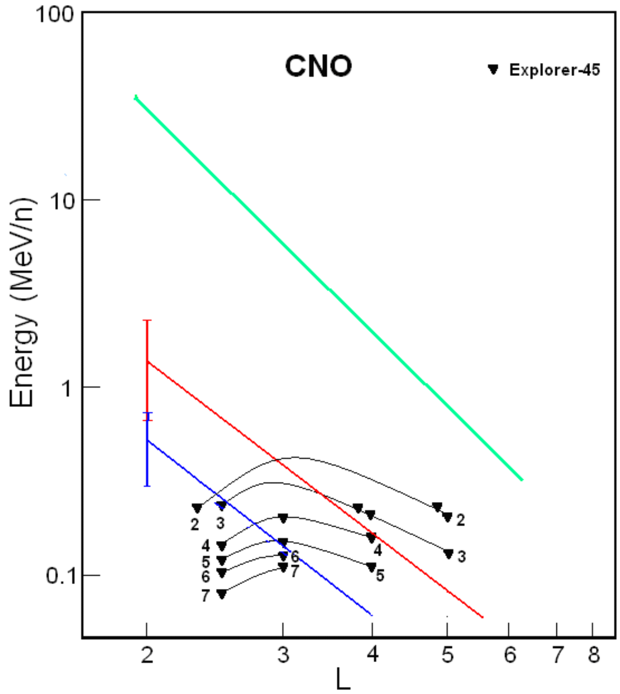

Figure 5. CNO ion fluxes in the ERB near the maximum of a solar activity. A numbers on the curves are equal the values of a decimal logarithms of J where J in (cm^2 s ster MэB/n)$^{-1}$ are differential flux of protons with $\alpha_0 \approx 90^{\circ}$ (near the plane of the geomagnetic equator). The data of different satellites presented by different symbols.

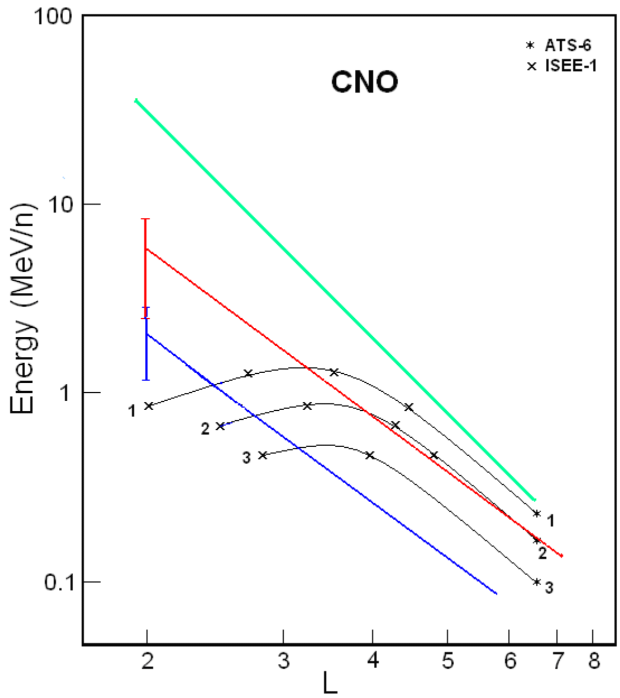

Figure 6. CNO ion fluxes in the ERB near the minimum of a solar activity. A numbers on the curves are equal the values of a decimal logarithms of J where J in (cm^2 s ster MэB/n)$^{-1}$ are differential flux of protons with $\alpha_0 \approx 90^{\circ}$ (near the plane of the geomagnetic equator). The data of different satellites presented by different symbols.

https://doi.org/10.5194/angeo-2019-82
Preprint. Discussion started: 13 June 2019

Annales Geophysicae Discussions Open Access EGU

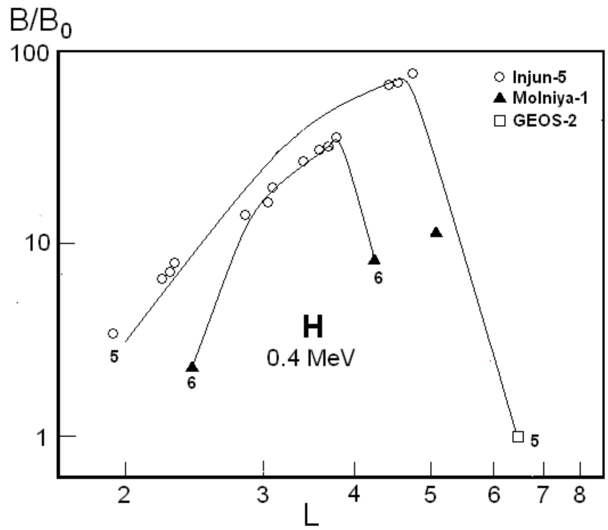

Figure 7. Average stationary fluxes of protons with $E = 0.4$ MeV in space $\{L, B/B_0\}$ near the maxima of solar activity. A numbers on the curves are equal the values of a decimal logarithms of J where J in $(\text{cm}^2 \text{ s ster MэB/n})^{-1}$. The data of different satellites presented by different symbols.

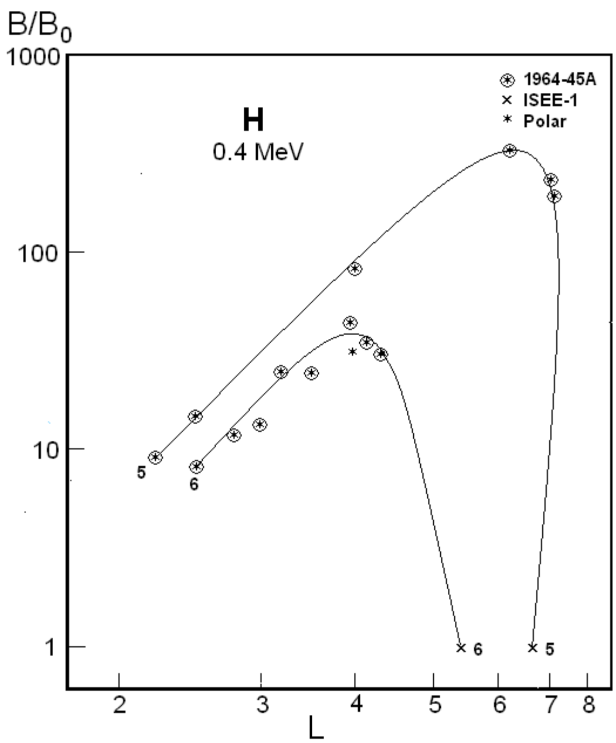

Figure 8. Average stationary fluxes of protons with $E = 0.4$ MeV in space $\{L, B/B_0\}$ near the minima of solar activity. A numbers on the curves are equal the values of a decimal logarithms of J where J in $(\text{cm}^2 \text{ s ster MэB/n})^{-1}$. The data of different satellites presented by different symbols.

https://doi.org/10.5194/angeo-2019-82
Preprint. Discussion started: 13 June 2019

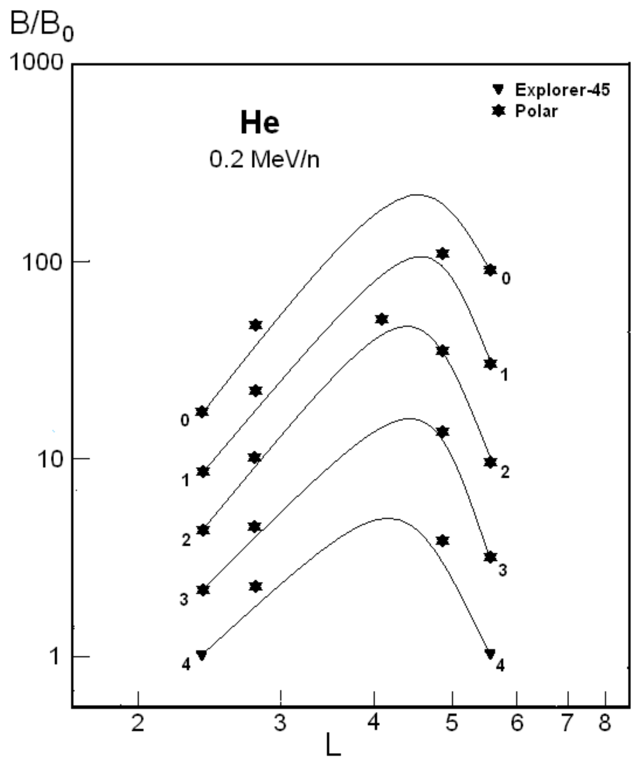

Figure 9. Average stationary fluxes of helium ions with E = 0.2 MeV/n in space $\{L, B/B_0\}$ near the minimum of a solar activity. A numbers on the curves are equal the values of a decimal logarithms of J where J in (cm^2 s ster MэB/n)$^{-1}$. The data of different satellites presented by different symbols.